Journal of Controlled Release 169 (2013) 296–305

Contents lists available at SciVerse ScienceDirect

Journal of Controlled Release

journal homepage: www.elsevier.com/locate/jconrel

Calcium depletion-mediated protease inhibition and apical-junctional-complex disassembly *via* an EGTA-conjugated carrier for oral insulin delivery

Er-Yuan Chuang [a,1], Kun-Ju Lin [b,c,1], Fang-Yi Su [a,1], Hsin-Lung Chen [a], Barnali Maiti [a], Yi-Cheng Ho [d], Tzu-Chen Yen [c], Nilendu Panda [a], Hsing-Wen Sung [a,*]

[a] Department of Chemical Engineering/Institute of Biomedical Engineering, National Tsing Hua University, Hsinchu, Taiwan, ROC
[b] Department of Medical Imaging and Radiological Sciences, Chang Gung University, Taoyuan, Taiwan, ROC
[c] Department of Nuclear Medicine and Molecular Imaging Center, Chang Gung Memorial Hospital, Taoyuan, Taiwan, ROC
[d] Department of Biotechnology, Vanung University, Chungli, Taoyuan, Taiwan, ROC

ARTICLE INFO

Article history:
Received 30 September 2012
Accepted 20 November 2012
Available online 27 November 2012

Keywords:
Oral protein delivery
Chelating agent
Calcium depletion
Enzyme inhibition
Apical junctional complex

ABSTRACT

Calcium (Ca^{2+}) has a crucial role in maintaining the intestinal protease activity and in forming the apical junctional complex (AJC) that preserves epithelial barrier function. Ethylene glycol tetraacetic acid (EGTA) is a Ca^{2+}-specific chelating agent. To maintain the concentration of this chelator in areas where enzyme inhibition and paracellular permeation enhancement are needed, this study synthesized a poly(γ-glutamic acid)–EGTA conjugate (γPGA–EGTA) to form nanoparticles (NPs) with chitosan (CS) for oral insulin delivery. The results of our molecular dynamic (MD) simulations indicate that Ca^{2+} ions could be specifically chelated to the nitrogen atoms, ether oxygen atoms, and carboxylate oxygen atoms in $[Ca(EGTA)]^{2-}$ anions. By chelating Ca^{2+}, γPGA–EGTA conferred a significant insulin protection effect against proteases in intestinal tracts isolated from rats. Additionally, calcium depletion by γPGA–EGTA could stimulate the endocytosis of AJC components in Caco-2 cell monolayers, which led to a reversible opening of AJCs and thus increased their paracellular permeability. Single-photon emission computed tomography images performed in the biodistribution study clearly show the ^{123}I-insulin orally delivered by CS/γPGA–EGTA NPs in the heart, aorta, renal cortex, renal pelvis and liver, which ultimately produced a significant and prolonged hypoglycemic effect in diabetic rats. The above results confirm that this γPGA–EGTA conjugate is a promising candidate for oral insulin delivery.

1. Introduction

Ease of administration coupled with high patient compliance makes the oral route the preferred mode of drug administration. However, the drawbacks of orally administered hydrophilic macromolecules include enzymatic degradation in the gastrointestinal (GI) tract and barrier to physical absorption in the epithelium [1]. To address these issues, we recently reported a pH-responsive nanoparticle (NP) system composed of chitosan (CS) and poly(γ-glutamic acid) conjugated with diethylene triamine pentaacetic acid (γPGA–DTPA) [2]. CS, a mucoadhesive polycation, enhances paracellular permeability by transiently opening tight junctions (TJs) between epithelial cells [3], whereas DTPA inhibits intestinal proteases and disrupts epithelial TJs by nonspecific chelation of divalent metal ions such as Ca^{2+}, Mg^{2+} and Zn^{2+} [4]. Our experimental results indicated that this CS/γPGA–DTPA NP system effectively enhances insulin absorption throughout the entire small intestine [2].

Studies showed that calcium (Ca^{2+}) has crucial roles in chymotrypsin activity and in maintaining the thermodynamic stability of trypsin [5,6]. Trypsin and chymotrypsin are the major proteolytic enzymes present in the intestinal lumen, where cleavage of insulin molecules occurs [7]. Extracellular Ca^{2+} is also required to form the apical junctional complex (AJC) needed for epithelial barrier function. Therefore, depletion of Ca^{2+} in the intestinal lumen is advantageous for oral administrated insulin to prevent enzymatic degradation and enhance penetration through intestinal epithelial cells.

EGTA, a Ca^{2+}-specific chelator, has significantly greater Ca^{2+} affinity compared to other chelating agents [8]. Due to its Ca^{2+}-binding specificity, EGTA is more favorable for oral insulin delivery than DTPA. To take advantage of its Ca^{2+}-binding specificity, an amine-group containing EGTA derivative was first synthesized and then conjugated on γPGA to form NPs with CS for oral insulin delivery. Structural changes in the as-prepared NPs were examined in different pH environments by dynamic light scattering (DLS), transmission electron microscopy (TEM), and small angle X-ray scattering (SAXS). Effects of γPGA–EGTA on enzymatic inhibition and on paracellular permeability were

* Corresponding author at: Department of Chemical Engineering, National Tsing Hua University, Hsinchu 30013, Taiwan, ROC. Tel.: +886 3 574 2504.
E-mail address: hwsung@che.nthu.edu.tw (H.-W. Sung).
[1] The first three authors (E.Y. Chuang, K.J. Lin and F.Y. Su) contributed equally to this work.

0168-3659/$ – see front matter © 2012 Elsevier B.V. All rights reserved.
http://dx.doi.org/10.1016/j.jconrel.2012.11.011

evaluated *in vitro* in isolated rat intestinal segments and in Caco-2 cell monolayers, respectively. Furthermore, the mechanism of TJ opening induced by test NPs was studied by visualizing the ultra-structural changes in the epithelial AJC *via* TEM and confocal laser scanning microscopy (CLSM). The biodistribution of insulin orally delivered by the developed NPs was investigated by single-photon emission computed tomography (SPECT); their pharmacokinetic (PK) and pharmacodynamic (PD) profiles were then analyzed in a diabetic rat model.

2. Materials and methods

2.1. Materials

The 85%-deacetylated CS (MW 60 kDa) was purchased from Koyo Chemical Co. (Japan), whereas γPGA (MW 100 kDa) was acquired from Vedan Co. (Taichung, Taiwan). Other chemicals and reagents used were of analytical grade and obtained from Sigma-Aldrich (St. Louis, MO, USA).

2.2. Synthesis and characterization of γPGA–EGTA

An amine-group containing EGTA derivative was first prepared by incorporating an amino-functionalized aromatic moiety on the oxoethylenic bridge of EGTA [9]. Briefly, ethanolamine (0.9 g) was reacted with $KHCO_3$ (3.8 g) and tert-butyl bromoacetate ($BrCH_2COO^tBu$, 7.4 g) in dimethylformamide (DMF, 25 mL) at room temperature for 24 h. The crude product in ethyl acetate (CH_3CO_2Et, 25 mL) was subsequently mixed with *N*,*N*-diisopropylethylamine (iPr_2NET, 2.2 g) and MsCl (1.9 g) and reacted for 24 h. The pure compound in DMF (15 mL) was then mixed with K_2CO_3 (1.6 g), NaI (1.8 g) and 4-nitrocatechol (0.8 g) and stirred for 24 h; the product was dissolved in methanol and hydrogenated with 10% Pd/C. The obtained EGTA derivative was purified by column chromatography and then conjugated on γPGA (the γPGA–EGTA conjugate, Fig. 1a) as described below.

The γPGA–EGTA conjugate was prepared by reacting the acid form of γPGA (0.1 g) with an equimolar amine-group of the EGTA derivative in the presence of 1-ethyl-3-(3-dimethylaminopropyl) carbodiimide hydrochloride (EDC, 0.2 g) and *N*-hydroxysuccinimide (NHS, 0.1 g) in dimethyl sulfoxide (DMSO) at room temperature for 48 h. The product was purified by dialysis against deionized (DI) water for 3 days and then lyophilized. The Boc-deprotection reaction was performed by mixing the freeze-dried product with trifluoroacetic acid (TFA, 5 mL) at room temperature for 48 h. Finally, the synthesized γPGA–EGTA conjugate was purified by dialysis against DI water for 3 days and lyophilized before further use.

The synthesized γPGA–EGTA conjugate was characterized by ^1H NMR (Varian Unityionva 500 NMR Spectrometer, MO, USA) and FT-IR (Perkin-Elmer Spectrum RX 1 FT-IR System, Buckinghamshire, UK). The degree of substitution (DS) of EGTA on γPGA was estimated by ^1H NMR spectroscopy. The Ca^{2+} binding efficiency of γPGA–EGTA was determined by complexometric titration [10].

The conformation of γPGA–EGTA in the presence of Ca^{2+} and Mg^{2+} was examined by molecular dynamic (MD) simulations [11].

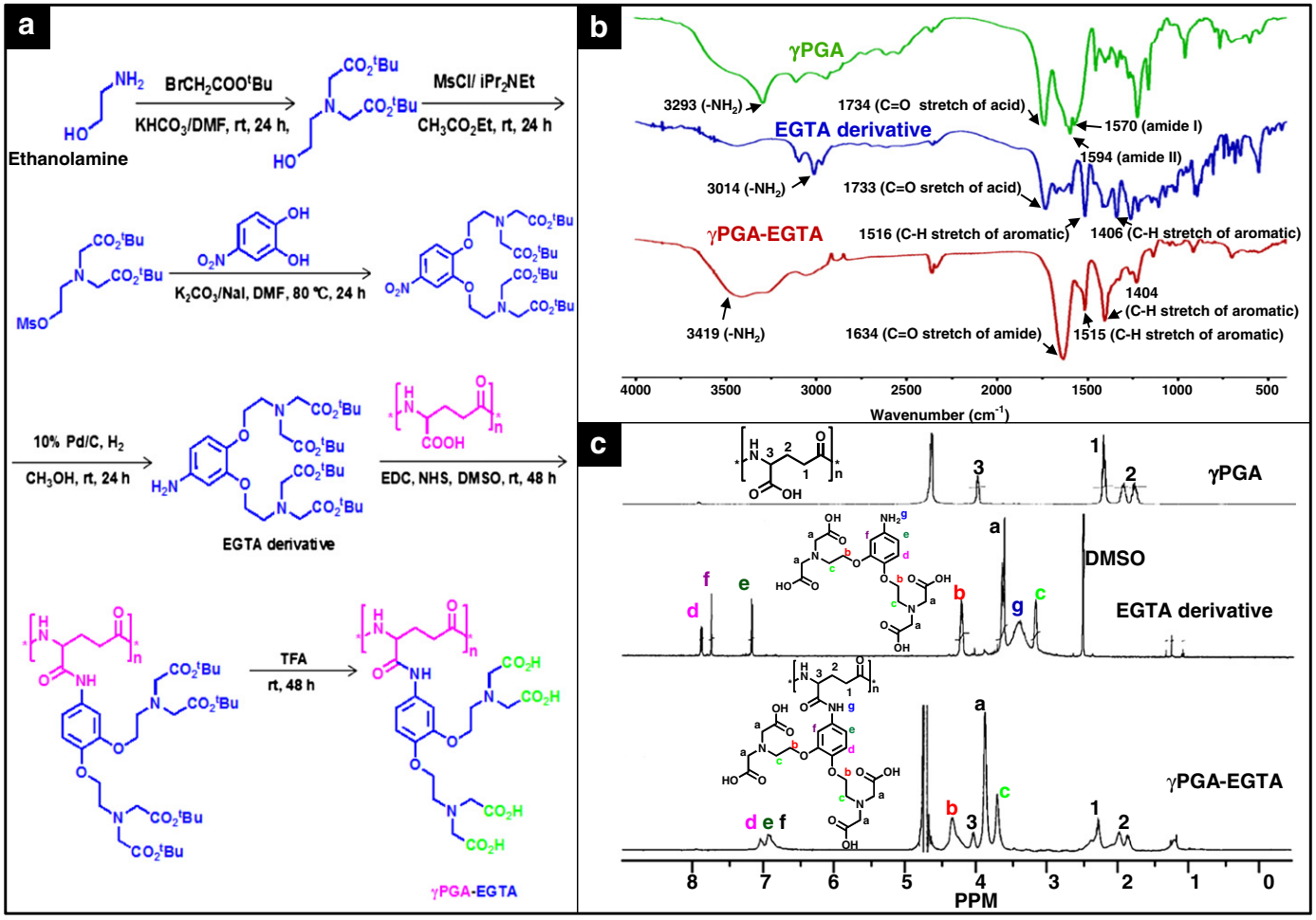

Fig. 1. Synthesis and characterization of the γPGA–EGTA conjugate: (a) the reaction scheme showing the formation of an amino-functionalized EGTA derivative and its subsequent conjugation on the γPGA backbone; (b) the FT-IR and (c) ^1H NMR spectra of the free-form γPGA, EGTA derivative and synthesized γPGA–EGTA conjugate. γPGA: poly(γ-glutamic acid) and EGTA: ethylene glycol tetraacetic acid.

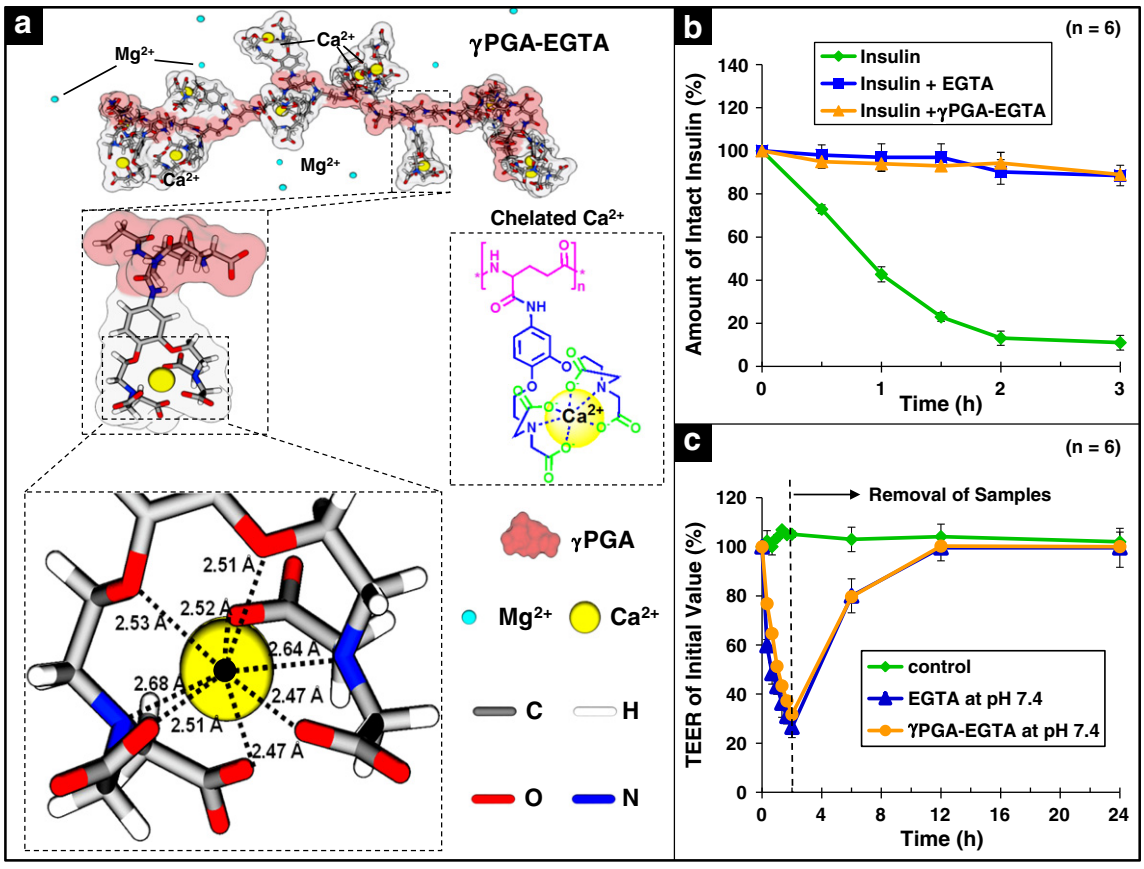

Fig. 2. (a) Results of molecular dynamic simulations showing the conformation of γPGA–EGTA in the presence of Ca^{2+} and Mg^{2+}; (b) effects of EGTA and γPGA–EGTA on insulin protection against intestinal proteases and (c) transepithelial electrical resistance (TEER) in Caco-2 cell monolayers. Control: the group without any treatment.

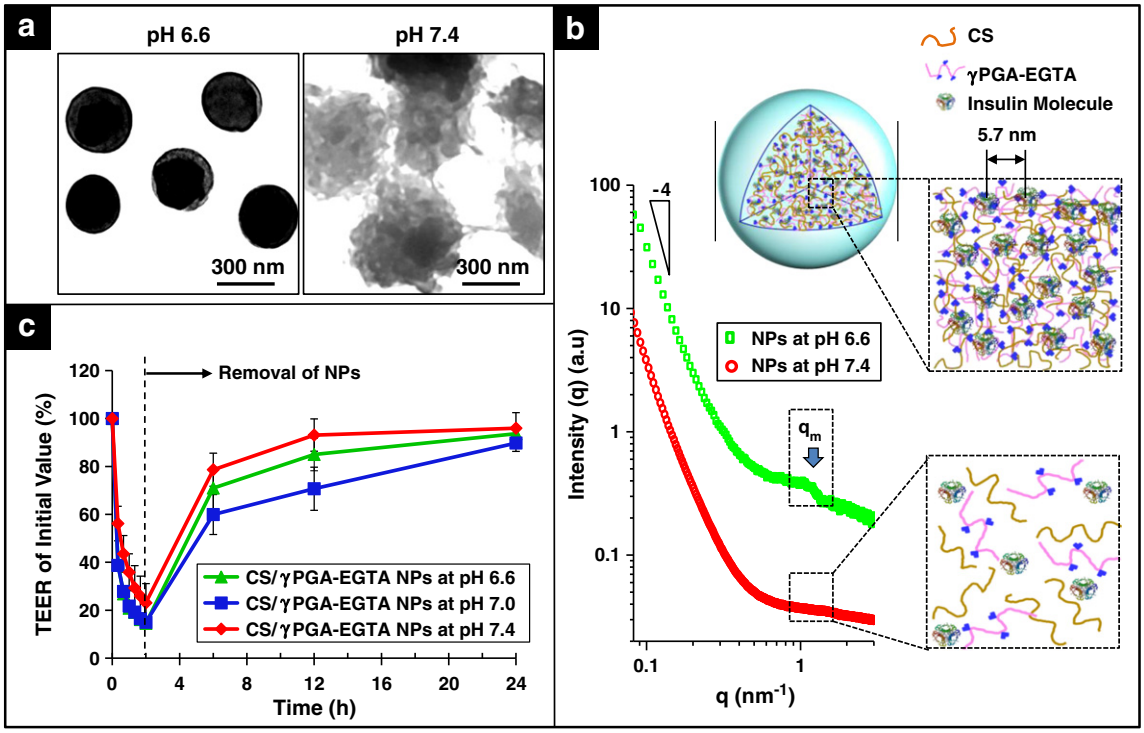

Fig. 3. (a) TEM micrographs and (b) small angle X-ray scattering (SAXS) profiles showing the pH-responsive characteristics of insulin-loaded CS/γPGA–EGTA nanoparticles (NPs); (c) effects of these NPs on the TEER of Caco-2 cell monolayers at distinct pH environments. CS: chitosan.

In body fluids, the predominant divalent metal ions are Ca^{2+} and Mg^{2+} [12], and Ca^{2+} and Mg^{2+} ion levels are higher in gastrointestinal (GI) mucosae than in blood [13,14]. Atomistic pictures of molecules were generated using UCSF Chimera.

2.3. Inhibition of intestinal proteolytic degradation

In vitro studies of intestinal protease inhibition by γPGA–EGTA were performed using proximal sections of small intestine freshly isolated from rats (Wistar, 180–200 g) [2]. The intestinal tissues were incubated with a Krebs–Ringer buffer (KRB) solution containing insulin (1 mg/mL, 1 mL) and γPGA–EGTA (5 mg/mL) at 37 °C; free-form EGTA (2 mg/mL) at 37 °C, which had a similar Ca^{2+} binding capacity, was used as a control. To quantify the amount of intact insulin remaining, test solutions (50 μL) withdrawn at different time intervals were immediately analyzed by high-performance liquid chromatography (HPLC).

2.4. Permeability of epithelial AJCs

The permeability of the epithelial AJCs in Caco-2 cell monolayers after treatment with test samples was measured in terms of transepithelial electrical resistance (TEER). The cell monolayers were incubated individually with EGTA (4 mg/mL, 0.5 mL) and γPGA–EGTA (10 mg/mL, 0.5 mL), which had equivalent Ca^{2+} binding capacities. The change of TEER for the tightness of cell monolayers was measured with a Millicell®-Electrical Resistance System (Millipore Corp., Bedford, MA, USA).

2.5. Preparation and characterization of CS/γPGA–EGTA NPs

A simple ionic-gelation method was used to prepare the insulin-loaded CS/γPGA–EGTA NPs [2]. The particle size and zeta potential of the prepared NPs were measured by DLS (3000 HS, Malvern Instruments Ltd., Worcestershire, UK), and morphology study was performed by TEM (JEOL 2010F, Tokyo, Japan). The loading efficiency (LE) and loading content (LC) of insulin in NPs were calculated using a method reported previously [15]. The internal structures of CS/γPGA–EGTA NPs were examined by SAXS [16] after resuspending the test NPs in phosphate buffered saline (PBS) of different pH values. Additionally, TEER measurements of Caco-2 cell monolayers incubated with CS/γPGA–EGTA NPs (0.02% w/v, 0.5 mL) were performed at pH values of 6.6, 7.0, or 7.4 (to simulate the pH environments in different portions of the small intestine) in the donor compartment and at pH 7.4 in the receiver compartment.

2.6. Ultra-structural changes in AJCs

After treating test NPs with EGTA conjugate (CS/γPGA–EGTA NPs, 0.2 mg/mL) or without EGTA conjugate (CS/γPGA NPs), ultra-structural changes in epithelial AJCs in Caco-2 cell monolayers were examined by TEM; paracellular permeability was then depicted by lanthanum nitrate staining. Lanthanum is an electron-dense rare-earth element widely used as a tracer for studying junctional barrier permeability [17]. The cell monolayers were fixed in 3.7% paraformaldehyde, washed with s-Collidine buffer, and incubated with 2% lanthanum for 2 h at room temperature. After rinsing in s-Collidine and PBS, samples were processed for TEM examination as detailed previously [18].

2.7. Translocation of AJC proteins

The Caco-2 cells were grown to confluence in 35-mm dishes with glass cover-slip bottoms and then treated with test NPs for 2 h; translocation of their AJC proteins was investigated by immunofluorescence staining. The treated cells were washed 3 times with pre-warmed PBS and then fixed and permeabilized in 100% acetone for 10 min at −20 °C. Non-specific binding was blocked in 5% normal goat serum (Jackson ImmunoResearch Laboratories, West Grove, PA, USA) in PBS for 60 min at 37 °C. The cells were then incubated overnight in primary antibodies [mouse anti-claudin-4 (Invitrogen) and donkey anti-E-cadherin (Abcam, Cambridge, MA, USA)] at 4 °C. The results were visualized by applying appropriate Alexa-Fluor-conjugated secondary antibodies (Invitrogen); the cells were also counterstained with SYTOX blue (Invitrogen) for examination by inverted CLSM.

Extracellular calcium levels were measured by staining the treated cells with 40 mM Alizarin Red S (ARS), pH 4.0, for 10 min, and then washing with 70% ethanol and then with PBS to remove non-specific staining [19]. Samples were then visualized by an inverted phase-contrast light microscope (Nikon Eclipse-Ti, Nikon Instruments Inc., Melville, NY, USA).

2.8. Animal study

Animal studies were performed according to the "Guide for the Care and Use of Laboratory Animals" prepared by the Institute of Laboratory Animal Resources, National Research Council and published by the National Academy Press, revised in 1996.

The biodistribution of insulin orally delivered by CS/γPGA-EGTA NPs was studied in rats (n = 3) by using SPECT. In the study, ^{123}iodine was used to radiolabel insulin (^{123}I-insulin) using iodogen precoated tubes (Thermo Fisher Scientific, Rockford, IL, USA). Following the last SPECT scan, additional whole-body CT images of the heart, lungs, great vessels, liver and kidneys were acquired after intravenous administration of the Conray™ contrast agent (Mallinckrodt, MO, USA). To maximize the amount of contrast fluid stasis in the vasculature, the contrast agent was slowly injected *via* the tail vein (2 mL over 40 s). After receiving half of the Conray™ dose, each animal was sacrificed by co-injection of potassium chloride under deep anesthesia. The detailed protocols used in the image scanning and its quantification were previously described by our group [20,21]. To calculate the percentage of initial dose (% ID) within each area, the corresponding volumes of interest (VOIs) were manually drawn on the co-registered reference CT and dynamic scintigraphic images. Biodistribution data were expressed as % ID using the following formula:

$$\%\ \mathrm{ID} = \frac{\text{decay corrected radioactivity within the VOI at each time frame} \times 100\%}{\text{whole body radioactivity at the 1st image frame}}.$$

Diabetes was induced in rats (Wistar, 250 g) *via* intraperitoneal injection of streptozotocin (STZ) as described previously [22]. The rats with induced diabetes were then fasted overnight and for the remainder of the experiment but with free access to water. The following formulations were administered individually to the diabetic rats: an enteric-coated capsule containing free-form insulin powder (30 IU/kg) and trehalose (oral); an enteric-coated capsule filled with CS/γPGA-EGTA NPs containing 30 IU/kg insulin (oral); and a subcutaneous (SC) injection of free-form insulin solution (5 IU/kg, n = 6 for each studied group). Blood sampling from the tail veins of rats was performed before administering the drug and at varying time intervals after dosing. The blood glucose levels were then measured with a glucose meter (LifeScan, Milpitas, CA, USA). Plasma

Table 1
Mean particle sizes (nm), polydisperse index, and zeta potential values (mV) of CS/γPGA–EGTA nanoparticles (NPs) at distinct pH environments (n = 5 batches). N/A: data were not available due to the observed disintegration of NPs.

pH value	Mean particle size	Polydisperse index	Zeta potential
6.0	328.6 ± 2.3	0.23 ± 0.02	38.7 ± 0.2
6.6	354.3 ± 3.1	0.25 ± 0.05	12.1 ± 0.4
7.0	1549.3 ± 33.9	0.39 ± 0.08	7.1 ± 0.6
7.4	N/A	0.48 ± 0.13	1.3 ± 0.9

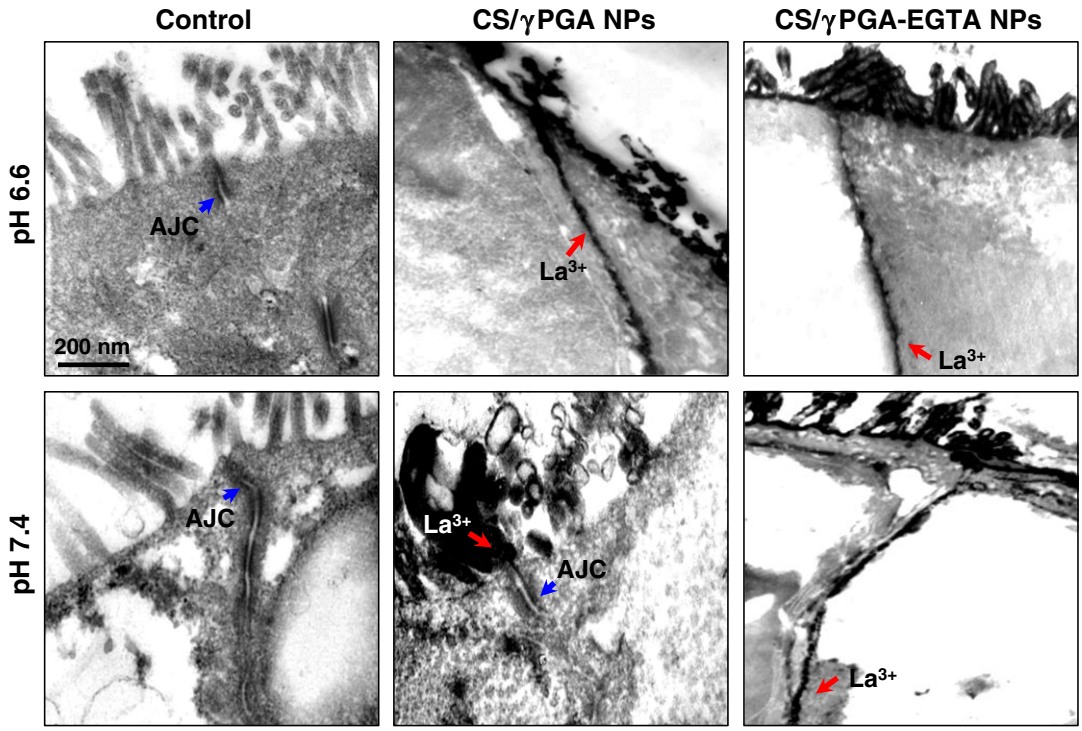

Fig. 4. TEM micrographs showing the effects of CS/γPGA NPs or CS/γPGA–EGTA NPs on the AJC opening and its subsequent paracellular permeability in the cell monolayers at pH 6.6 and 7.4. AJC: apical junctional complex; blue arrow: indicating an intact AJC, and red arrow: indicating the lanthanum (La^{3+}) permeability through the opened intercellular spaces.

insulin levels and the relative bioavailability (BA_R) of insulin after oral administration were calculated using the following formula [16].

$$BA_R = \frac{AUC_{(oral)} \times Dose_{(SC)}}{AUC_{(SC)} \times Dose_{(oral)}} \times 100\%$$

where AUC is the total area under the plasma insulin concentration *versus* time curve.

2.9. Statistical analysis

The two groups were compared by using statistical software (SPSS, Chicago, Ill) to perform one-tailed Student *t*-test. All data were expressed as means with standard deviations indicated (mean ± SD). A difference of $P<0.05$ was considered statistically significant.

3. Results and discussion

Calcium depletion by chelating agents such as EGTA is known to increase paracellular permeability [23] and has a crucial role in inhibiting intestinal enzyme activities [24]. The EGTA, a hexadentate ligand, is best known for its selectivity for Ca^{2+} over Mg^{2+} (*ca.* 10^6-fold) [25]. In intestinal pH environments (pH 6.4–7.4), acidic groups of EGTA are deprotonated, which accelerates the association kinetics of Ca^{2+} [26].

To concentrate the chelating agent in areas where paracellular permeation enhancement and enzyme inhibition are needed, immobilization of this auxiliary agent on the drug-carrier matrix is crucial [27]. Our approach is to synthesize a γPGA–EGTA conjugate (Fig. 1a) to form NPs with CS for oral insulin delivery. Such a delivery system can concentrate the activities of permeation enhancement and enzyme inhibition in areas where drug release occurs in the intestinal mucus layer. This study shows that this CS/γPGA–EGTA NP system inhibits intestinal proteolytic degradation and promotes insulin absorption by the small intestine, thus enhancing the bioavailability of insulin.

3.1. Synthesizing and characterizing γPGA–EGTA

Fig. 1b shows the FT-IR spectra of free-form γPGA, the synthesized EGTA derivative, and γPGA–EGTA. The γPGA spectra exhibited absorbance peaks at 1734 cm^{-1} for carboxyl groups, 1594 cm^{-1} for amide II, and 1570 cm^{-1} for amide I, while those of the EGTA derivative showed absorbance peaks characteristic of –COOH (1733 cm^{-1}) and aromatic C–H stretching (1516 and 1406 cm^{-1}). For γPGA–EGTA, the presence of the peaks for amide bond (1634 cm^{-1}) and aromatic C–H stretching (1515 and 1404 cm^{-1}) confirms the successful conjugation of EGTA derivative on γPGA.

In further analysis of the synthesized γPGA–EGTA by ^1H NMR (Fig. 1c), the spectrum of the unmodified γPGA displayed chemical shifts characteristic of α-CH ($\delta = 4.01$ ppm), β-CH_2 ($\delta = 1.96$ and 1.83 ppm) and γ-CH_2 ($\delta = 2.22$ ppm) while that of the EGTA derivative showed shifts indicating aromatic phenyl (7.87, 7.74 and 7.16 ppm) and methylene and primary amine protons (4.21, 3.16, 3.63 and 3.38 ppm). In the γPGA–EGTA conjugate, the characteristic peaks for aromatic protons (7.03 and 6.93 ppm) and methylene protons (4.31, 3.68 and 3.85 ppm) were for EGTA derivative, and those for α-CH ($\delta = 4.02$ ppm), β-CH_2 ($\delta = 1.95$ ppm and 1.83 ppm), and γ-CH_2 ($\delta = 2.25$ ppm) were from γPGA. These ^1H NMR results confirm the successful conjugation of the EGTA derivative on the γPGA backbone. According to the ^1H NMR spectrum of γPGA–EGTA, the DS of EGTA derivative on γPGA was an estimated 50%, which indicated the presence of 0.5 mol of EGTA for each mole of γPGA monomer.

The complexometric titration results showed that the Ca^{2+}-binding capacity of γPGA–EGTA at neutral pH (simulating the intestinal pH environment) was 1666.7 ± 8.3 μmol/g conjugate ($n = 6$), which was equivalent to an EGTA-to-Ca^{2+} molar ratio of 1:1. The chelation of Ca^{2+} by γPGA–EGTA results from proton release from the EGTA structure at neutral pH [26,28].

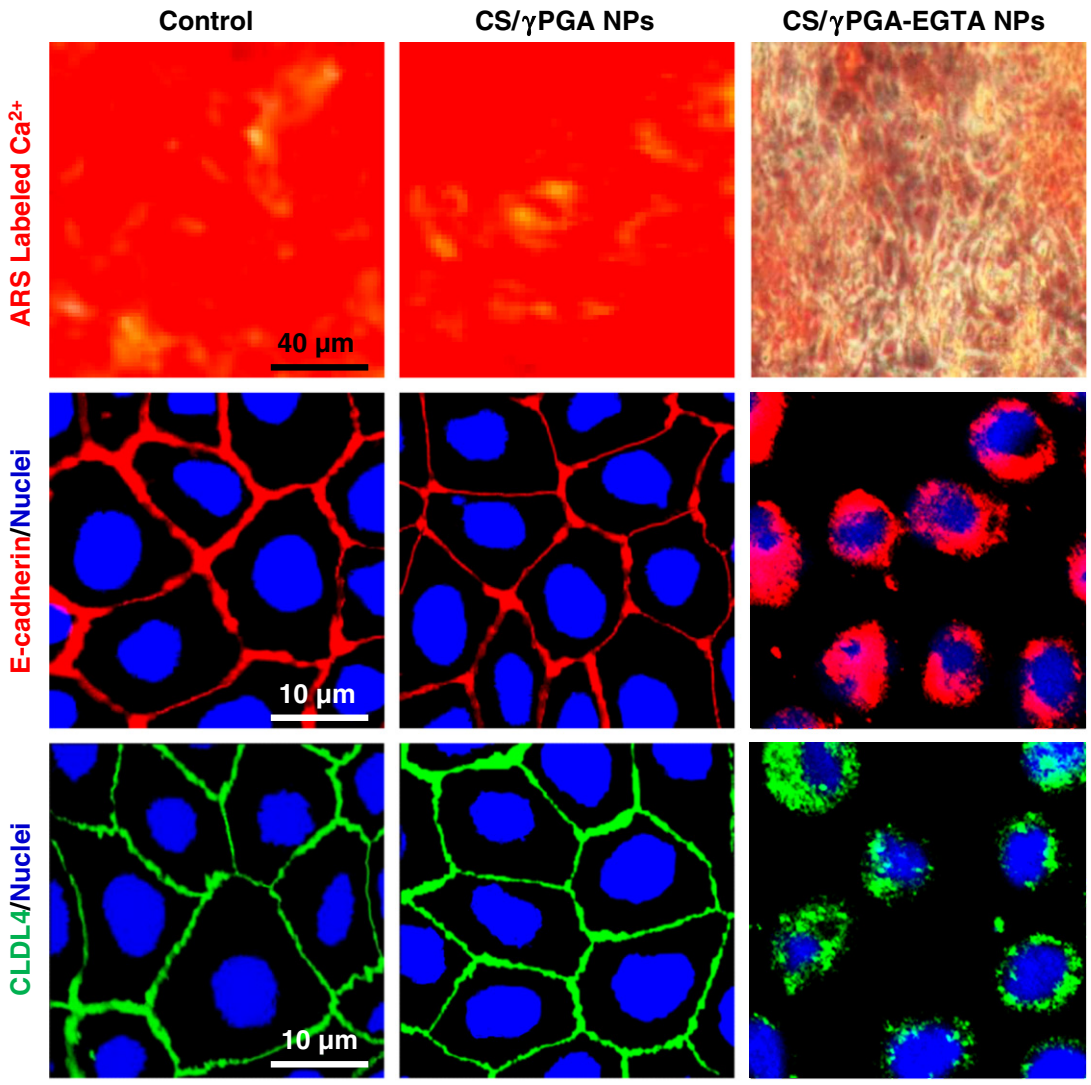

Fig. 5. Photomicrographs showing the extracellular calcium levels (as indicated by the red ARS-labeled Ca^{2+}) and the immunofluorescence staining of the cell monolayers before and after receiving CS/γPGA NPs or CS/γPGA–EGTA NPs at pH 7.4. ARS: Alizarin Red S.

The EGTA reportedly has a high binding affinity for Ca^{2+} (stability constant log K = 11.0) and a relatively low affinity for Mg^{2+} (log K = 5.2) [29]. The confirmation of the γPGA–EGTA chelated with Ca^{2+} ions alone, obtained by MD simulations, is shown in Fig. 2a. The Ca^{2+} in $[Ca(EGTA)]^{2-}$ anions binds to the nitrogen atoms (Ca–N), ether oxygen atoms (Ca–O), and carboxylate oxygen atoms (Ca–O) at average distances of 2.66 Å, 2.49 Å, and 2.52 Å, respectively. The Ca^{2+}/Mg^{2+} discrimination of EGTA presumably stems from its binding cavity, which is the right size for Ca^{2+} but does not further envelop Mg^{2+} tightly because the carboxylate anions at each end of the chain begin butting into each other [30]. The DTPA has similar stability constants for Ca^{2+} (log K = 10.7) and Mg^{2+} (log K = 9.3) [29] and therefore can chelate both Ca^{2+} and Mg^{2+} ions [4].

3.2. Inhibition of intestinal enzyme degradation by γPGA–EGTA

Insulin is very sensitive to trypsin and chymotrypsin, which are Ca^{2+}-dependent enzymes present in the intestinal fluid and mucus layer [31–33]. One strategy for inhibiting intestinal enzyme activities is removing essential metal ions such as Ca^{2+} from the enzyme structure [24]; the affinity for Ca^{2+} correlates with the strength of the enzyme inhibition. The inhibitory activity of γPGA–EGTA against intestinal proteases was investigated in proximal intestinal tracts freshly isolated from rats and placed in KRB, a simulated intestinal fluid [34].

Fig. 2b shows that the control group of free-form insulin was rapidly degraded by the intestinal proteolytic enzymes (approximately 90% insulin degradation within 3 h). Adding EGTA, or γPGA–EGTA conferred a significant protective effect of insulin against proteases ($P<0.05$). EGTA and γPGA–EGTA conferred much larger insulin protection effects compared to their DTPA counterparts reported in our previous study (8% *vs.* 35% insulin degradation, respectively $P<0.05$) [2]. These experimental results confirm that EGTA and γPGA–EGTA are superior to their DTPA counterparts in terms of enzyme inhibition as they have specific capability to deprive Ca^{2+} from the structure of enzymes, which ultimately helps prevent insulin degradation.

3.3. Enhancement of the paracellular permeability

Calcium is critical for maintaining cell–cell junctions in various cell types [35]. The use of complexing agents for chelating extracellular Ca^{2+} can disrupt intercellular junctions and can increase paracellular permeability. The well-established *in vitro* Caco-2 cell model was used to evaluate absorption enhancement across the intestinal epithelium by assessing their TEER [36]. Fig. 2c shows that Caco-2 cell monolayers treated with free-form EGTA or γPGA–EGTA produced a

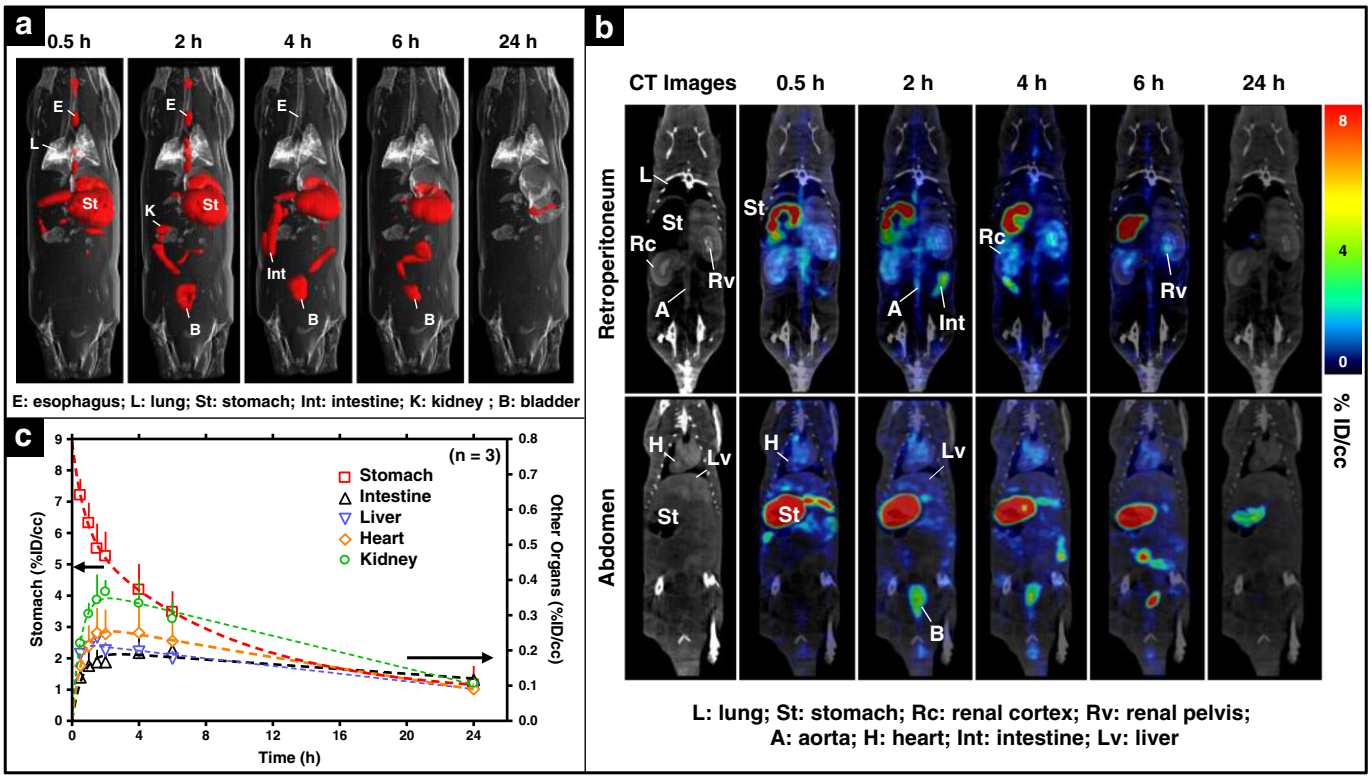

Fig. 6. (a) Soft-tissue contrast CT images (in gray) superimposed with 3D volume-rendering SPECT images (in red) showing the distribution of ^{123}I-insulin in various body compartments obtained at different time points; (b) biodistribution of ^{123}I-insulin illustrated by contrast-enhanced tomographic images. The concentrations of ^{123}I-insulin in different organs are shown in rainbow pseudo-color scale and (c) their percentages of ingested dose per volume (% ID/cm^3) *vs.* time profiles of ^{123}I-insulin in the stomach (left y-axis) and other organs (right y-axis) are also demonstrated.

significantly larger reduction in TEER compared to the control cells ($P<0.05$). The TEER reduction induced by EGTA and γPGA–EGTA was larger than that induced by their DTPA counterparts [2]. Again, the larger reduction may have resulted from their binding specificity towards Ca^{2+}. After removing the test samples and replenishing the medium, TEER increased gradually and recovered almost completely within 24 h, indicating that the transient calcium depletion may allow a reversible modulation of paracellular permeability.

3.4. Characteristics of CS/γPGA–EGTA NPs

The CS/γPGA–EGTA NPs prepared in DI water (pH 6.0) had a particle size of 328.6 ± 2.3 nm and a zeta potential of 38.7 ± 0.2 mV; their insulin LE and LC were 78.7 ± 0.4% and 17.5 ± 1.5%, respectively (n = 5 batches). The pH-sensitivity of test NPs was evaluated at distinct pH environments, representing the small intestine conditions. As pH was increased, the size of the test NPs significantly increased until they eventually disintegrated at pH 7.4 (Fig. 3a); however, their zeta potential values significantly decreased ($P<0.05$, Table 1) due to CS deprotonation.

Fig. 3b shows the SAXS profiles in a log–log plot of CS/γPGA–EGTA NPs dispersed in different pH environments. Close study of the SAXS profiles of test NPs at pH 6.6 showed peak centering at about 1.1 nm^{-1}. Earlier, the authors showed that this peak is attributable to the characteristic correlation between the insulin molecules contained within the individual NP [18], where the relatively high concentration of insulin molecules in test NPs produces an interaction peak. The characteristic correlation distance between the insulin molecules calculated from the peak position *via* $d = 2\pi/q_m$ approximated 5.7 nm. No scattering peak occurred when the pH of the medium was increased to 7.4. At this pH value, the disintegrating test NPs released their originally embedded insulin molecules to the bulk media because CS deprotonation weakened their electrostatic attraction to γPGA–EGTA. Since most of the insulin molecules were not contained in the NPs, their spatial correlation peak was no longer observable in the SAXS profile.

Fig. 3c shows the TEER variations observed in the Caco-2 cell monolayers after receiving CS/γPGA–EGTA NPs at pH 6.6, 7.0 or 7.4. Regardless of pH exposure, all groups showed remarkably decreased TEER, indicating that the EGTA-conjugated NPs developed in the study may facilitate paracellular permeation in the pH environments from the proximal duodenum to the distal ileum (pH 6.4–7.4) along the intestinal tract. Conversely, the CS is well known to be inadequate for opening intercellular TJs in neutral pH environments [37], which limits its potential use as a permeation enhancer only in the duodenum section.

3.5. Ultra-structural study of AJC opening and paracellular permeability

Ultra-structural study of the AJC opening and its subsequent paracellular permeability in the cell monolayers was performed by TEM after treatment with CS/γPGA NPs or CS/γPGA–EGTA NPs at pH 6.6 and 7.4. Lanthanum (La^{3+}) was used as the electron microscopic stain because its interaction with negatively charged cell-surface glycoproteins makes it effective for delineating intercellular spaces [17].

Fig. 4 shows that before treatment with test NPs (controls), the intact AJCs (as pointed by the blue arrow) appeared as highly electron-dense structures underneath the apical cell membrane and between adjacent cells. When treated with the test NPs without EGTA conjugate (CS/γPGA NPs) at pH 6.6, lanthanum staining of the paracellular spaces between adjacent cells was clearly observed (red arrow), suggesting the opening of intercellular junctions mediated by CS [18]. At pH 7.4, the AJCs remained intact, and limitation of the lanthanum staining to the brush-border surface suggested that CS/γPGA NPs do not effectively enhance permeation at neutral pH values. Whereas CS (p*Ka* 6.5) facilitates paracellular transport only

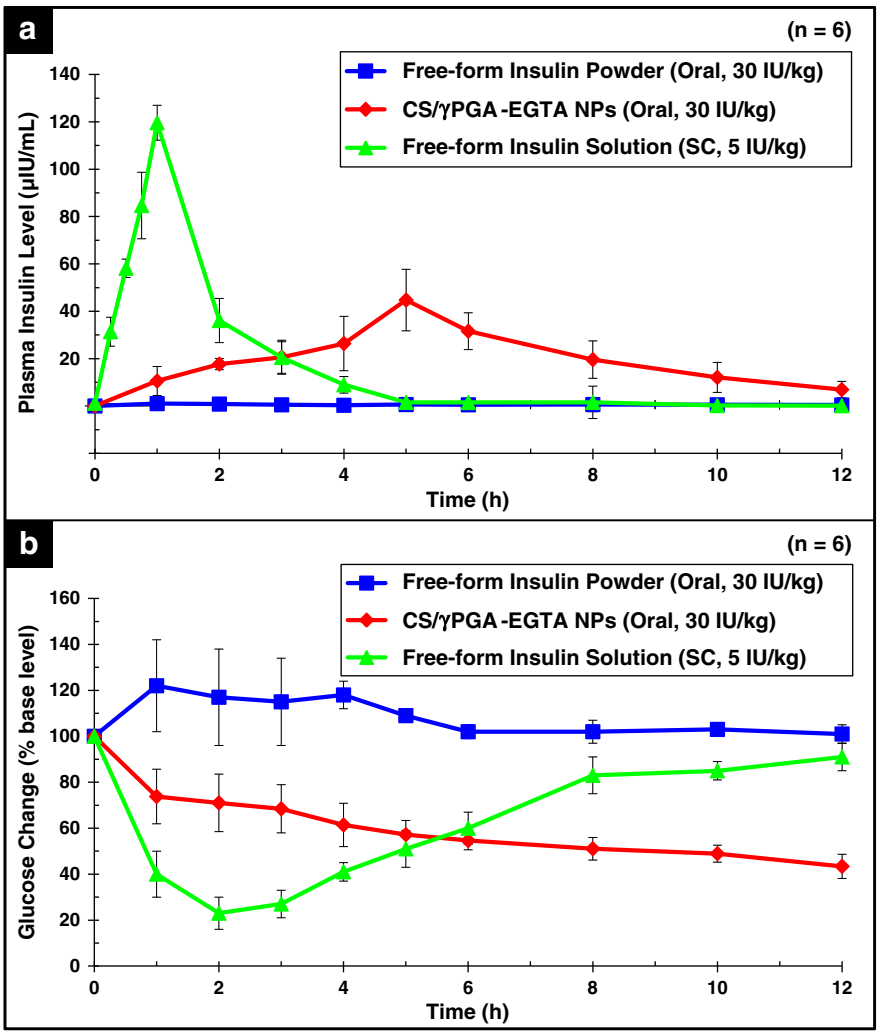

Fig. 7. (a) Plasma insulin level *vs.* time profiles and (b) blood glucose change *vs.* time profiles of diabetic rats treated with different formulations of insulin. Oral: oral administration and SC: subcutaneous injection.

after protonation [3], treatment with the EGTA-conjugated (CS/γPGA–EGTA) NPs caused the opening of AJCs and significant penetration of lanthanum into the lateral intercellular spaces at both test pH environments, possibly due to the deprivation of extracellular Ca^{2+} by EGTA. Calcium depletion by EGTA reportedly increases paracellular permeability [29].

3.6. AJC disassembly induced by calcium depletion

The AJC, which is comprised of adherens junctions (AJs) and TJs, is an important regulator of cell structure and function [38]. AJs bring two plasma membranes together physically and enhance TJ assembly; thus, alteration of AJs modulates the TJ structure and the epithelial paracellular barrier function. *E-cadherin*, a Ca^{2+}-dependent adhesion molecule, is the major *trans-membrane protein* of AJs, and claudin-4 (CLDN4) is a TJ protein [3,39]. Neither AJs nor TJs have a static structure; they can be rapidly disassembled and reorganized in response to various extracellular stimuli.

Fig. 5 shows the extracellular calcium levels (as indicated by the red ARS-labeled Ca^{2+}) and the immunofluorescence staining of the cell monolayers before and after receiving CS/γPGA NPs or CS/γPGA–EGTA NPs at pH 7.4. Extracellular Ca^{2+} is essential for AJC formation and for maintaining cell–cell junctions [40]. Compared to the control group, treatment with test NPs without EGTA conjugate (CS/γPGA NPs) did not significantly affect either extracellular calcium levels or translocation of E-cadherin and CLDN4.

In contrast, treatment with EGTA-conjugated NPs (CS/γPGA–EGTA NPs) substantially diminished extracellular calcium levels; additionally, internalization of both E-cadherin (red color) and CLDN4 (green color) to a cytosolic compartment surrounding the nucleus suggested that calcium depletion by EGTA stimulates endocytosis of AJC components. Internalization of AJs and TJs *via* a clathrin-dependent pathway appears to be a common mechanism to rapidly modulate the cell–cell sealing, which has been documented in the literature [40].

3.7. Biodistribution of insulin

Fig. 6a presents the radioactivity distribution of ^{123}I-insulin orally delivered by CS/γPGA–EGTA NPs over the 24-h period after ingestion in a rat model. The 3D volume-rendering SPECT images of ^{123}I-insulin (in red) were superimposed onto the soft-tissue contrast-volume-rendering CT images (in gray). Air in the hollow organs, including the bilateral lungs, stomach and intestine, was clearly visible in the volume-rendering CT images, whereas ^{123}I-insulin was identified in the GI track, kidneys and bladder *via* the SPECT images.

Additional details of the biodistribution of ^{123}I-insulin are visible in the coronal tomographic images (Fig. 6b), in which the radioactivity concentration of ^{123}I-insulin is presented in rainbow pseudo-color scale and superimposed on the CT images to distinguish anatomic

Table 2
Pharmacokinetic parameters of insulin in diabetic rats after subcutaneous (SC) administration of free-form insulin solution, oral administration of capsules containing free-form insulin powder or insulin-loaded CS/γPGA–EGTA NPs. C_{max}: maximum plasma concentration; T_{max}: time at which C_{max} is attained; $AUC_{(0-12\ h)}$: area under the plasma concentration–time curve; BA_R: relative bioavailability (n = 6).

	SC free-form insulin solution	Oral free-form insulin powder	Oral CS/γPGA–EGTA NPs
Dose (IU/kg)	5.0	30.0	30.0
C_{max} (μIU/mL)	119.63 ± 3.8	1.8 ± 0.7	44.7 ± 13.0
T_{max} (h)	1.0	5.0	5.0
$AUC_{(0-12\ h)}$ (μIU h/mL)	191.31 ± 30.7	6.5 ± 2.7	244.5 ± 33.7
BA_R (%)	100	0.5 ± 0.3	21.3 ± 1.5

localizations. The vascular structures, including the heart, aorta, renal cortex, renal pelvis and liver were visible in the contrast-enhanced CT images, while ^{123}I-insulin was clearly recognizable in the above-mentioned organs in the SPECT images. Fig. 6c shows the radioactivity concentrations of ^{123}I-insulin (% ID/cm^3) observed in different organs. After ingestion, the radioactivity concentration of ^{123}I-insulin present in the stomach diminished gradually, while those in the intestine, liver, heart and kidneys increased with time, reaching their maximum values at 3–4 h following ingestion, revealing the absorption of insulin into the systemic circulation.

3.8. In vivo PK and PD profiles

The SC injection of free-form insulin solution resulted in a maximum plasma concentration at 1 h post administration. Blood glucose levels then sharply decreased within 1–3 h before returning to their basal levels (Fig. 7a and b). Subsequent oral administration of capsules containing free-form insulin powder produced negligible insulin absorption and hypoglycemic effects. Conversely, administration of capsules containing insulin-loaded CS/γPGA–EGTA NPs produced a slow but prolonged reduction in blood glucose levels, indicating that the pharmacological activity of the absorbed insulin was still intact; their $AUC_{(0-12\ h)}$ was 244.5 ± 33.7 μIU h/mL, and the corresponding BA_R was 21.3 ± 1.5% (Table 2).

3.9. Functionality of γPGA–EGTA

Fig. 8 schematically depicts the functionality of γPGA–EGTA in facilitating oral insulin delivery according to the above results. By specific deprivation of extracellular Ca^{2+} from the intestinal lumen (Figs. 2a and 5), γPGA–EGTA can significantly reduce the enzymatic degradation of insulin (Fig. 2b). Additionally, *via* causing the endocytosis AJCs (Fig. 5), γPGA–EGTA displays the ability to modulate the transepithelial resistance (Fig. 2c), enhance the paracellular permeation (Fig. 4), and promote the insulin absorption (Fig. 6a–c), thus increasing its oral bioavailability (Fig. 7a and b).

4. Conclusions

A calcium-specific depletion agent, γPGA–EGTA, was successfully synthesized to formulate a carrier for oral insulin delivery. Our results indicate that γPGA–EGTA plays a significant role in the prevention of enzymatic degradation of insulin and in the enhancement of its paracellular permeability through the modulation of epithelial AJC disassembly, ultimately producing a significant and prolonged hypoglycemic effect. These results confirm the efficacy of the proposed EGTA-conjugated carrier in promoting the bioavailability of orally administered insulin.

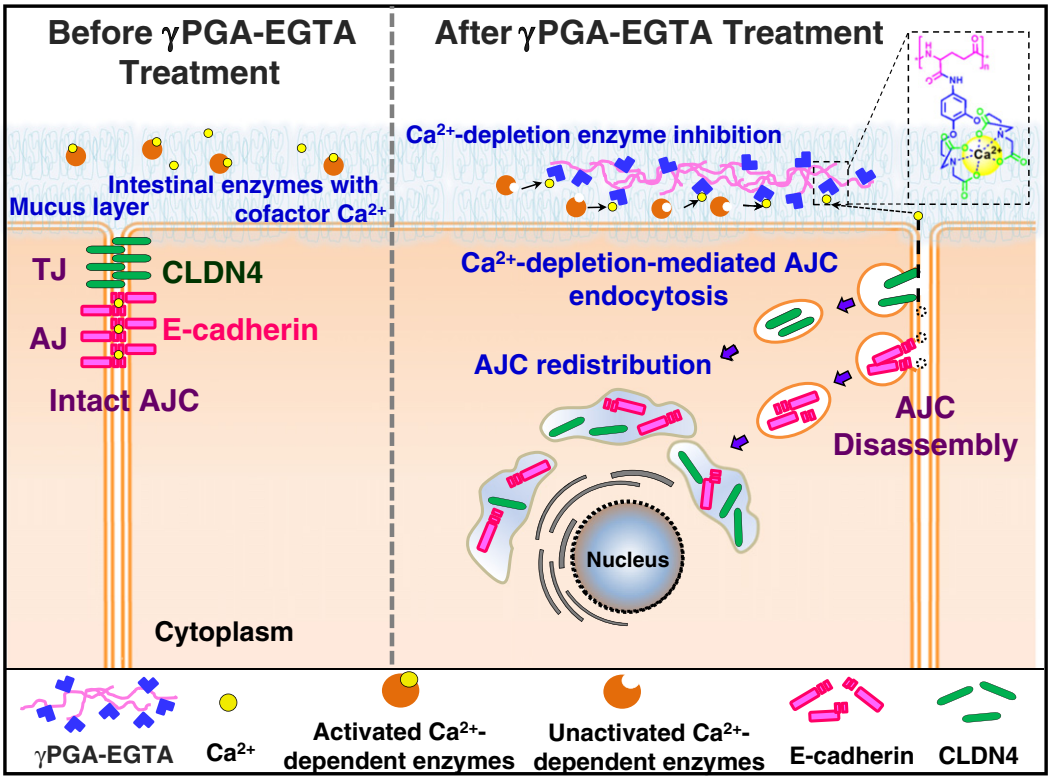

Fig. 8. Schematic illustrations displaying the specific deprivation of extracellular Ca^{2+} from the intestinal lumen by γPGA–EGTA and its subsequent effects on the inhibition of intestinal proteases and the enhancement of paracellular permeation.

Acknowledgments

This work was supported by a grant from the National Science Council (NSC 100-2120-M-007-003), Taiwan, Republic of China. The molecular-imaging study was partially supported by a grant from Chang Gung Memorial Hospital (CMRPG391512).

References

[1] C. Damge, P. Maincent, N. Ubrich, Oral delivery of insulin associated to polymeric nanoparticles in diabetic rats, J. Control. Release 117 (2007) 163–170.
[2] F.Y. Su, K.J. Lin, K. Sonaje, S.P. Wey, T.C. Yen, Y.C. Ho, N. Panda, E.Y. Chuang, B. Maiti, H.W. Sung, Protease inhibition and absorption enhancement by functional nanoparticles for effective oral insulin delivery, Biomaterials 33 (2012) 2801–2811.
[3] T.H. Yeh, L.W. Hsu, M.T. Tseng, P.L. Lee, K. Sonjae, Y.C. Ho, H.W. Sung, Mechanism and consequence of chitosan-mediated reversible epithelial tight junction opening, Biomaterials 32 (2011) 6164–6173.
[4] L. Shen, H.Y. Zhao, J. Du, F. Wang, Anti-tumor activities of four chelating agents against human neuroblastoma cells, In Vivo 19 (2005) 233–236.
[5] M. Morishita, T. Goto, N.A. Peppas, J.I. Joseph, M.C. Torjman, C. Munsick, K. Nakamura, T. Yamagata, K. Takayama, A.M. Lowman, Mucosal insulin delivery systems based on complexation polymer hydrogels: effect of particle size on insulin enteral absorption, J. Control. Release 97 (2004) 115–124.
[6] F.C. Wu, M. Laskowski, The effect of calcium on chymotrypsins [alpha] and B, Biochim. Biophys. Acta 19 (1956) 110–115.
[7] R.J. Schilling, A.K. Mitra, Degradation of insulin by trypsin and alpha-chymotrypsin, Pharm. Res. 8 (1991) 721–727.
[8] C.C. Kim, S. Falkow, Delineation of upstream signaling events in the salmonella pathogenicity island 2 transcriptional activation pathway, J. Bacteriol. 186 (2004) 4694–4704.
[9] L. Tei, Z. Baranyai, M. Botta, L. Piscopo, S. Aime, G.B. Giovenzana, Synthesis and solution thermodynamic study of rigidified and functionalised EGTA derivatives, Org. Biomol. Chem. 6 (2008) 2361–2368.
[10] A. Bernkop-Schnurch, C. Paikl, C. Valenta, Novel bioadhesive chitosan–EDTA conjugate protects leucine enkephalin from degradation by aminopeptidase N, Pharm. Res. 14 (1997) 917–922.
[11] Z.X. Liao, S.F. Peng, Y.C. Ho, F.L. Mi, B. Maiti, H.W. Sung, Mechanistic study of transfection of chitosan/DNA complexes coated by anionic poly(γ-glutamic acid), Biomaterials 33 (2012) 3306–3315.
[12] C. Leypold, M. Reiher, G. Brehm, M. Schmitt, S. Schneider, P. Matousek, M. Towrie, Tetracycline and derivatives—assignment of IR and Raman spectra via DFT calculations, Phys. Chem. Chem. Phys. 5 (2003) 1149–1157.
[13] X. Wang, Aspirin-like drugs cause gastrointestinal injuries by metallic cation chelation, Med. Hypotheses 50 (1998) 227–238.
[14] M. Cassidy, C. Tidball, Calcium and magnesium contents of gastrointestinal tissues in six species, Am. J. Physiol. 217 (1969) 674–679.
[15] Y.H. Lin, K. Sonaje, K.M. Lin, J.H. Juang, F.L. Mi, H.W. Yang, H.W. Sung, Multi-ion-crosslinked nanoparticles with pH-responsive characteristics for oral delivery of protein drugs, J. Control. Release 132 (2008) 141–149.
[16] K. Sonaje, Y.J. Chen, H.L. Chen, S.P. Wey, J.H. Juang, H.N. Nguyen, C.W. Hsu, K.J. Lin, H.W. Sung, Enteric-coated capsules filled with freeze-dried chitosan/poly([gamma]-glutamic acid) nanoparticles for oral insulin delivery, Biomaterials 31 (2010) 3384–3394.
[17] A.N. Flynn, O.A. Itani, T.O. Moninger, M.J. Welsh, Acute regulation of tight junction ion selectivity in human airway epithelia, Proc. Natl. Acad. Sci. U. S. A. 106 (2009) 3591.
[18] K. Sonaje, K.J. Lin, M.T. Tseng, S.P. Wey, F.Y. Su, E.Y. Chuang, C.W. Hsu, C.T. Chen, H.W. Sung, Effects of chitosan-nanoparticle-mediated tight junction opening on the oral absorption of endotoxins, Biomaterials 32 (2011) 8712–8721.
[19] Y. Zhang, J.R. Venugopal, A. El-Turki, S. Ramakrishna, B. Su, C.T. Lim, Electrospun biomimetic nanocomposite nanofibers of hydroxyapatite/chitosan for bone tissue engineering, Biomaterials 29 (2008) 4314–4322.
[20] K. Sonaje, K.J. Lin, S.P. Wey, C.K. Lin, T.H. Yeh, H.N. Nguyen, C.W. Hsu, T.C. Yen, J.H. Juang, H.W. Sung, Biodistribution, pharmacodynamics and pharmacokinetics of insulin analogues in a rat model: oral delivery using pH-Responsive nanoparticles vs. subcutaneous injection, Biomaterials 31 (2010) 6849–6858.
[21] H.N. Nguyen, S.P. Wey, J.H. Juang, K. Sonaje, Y.C. Ho, E.Y. Chuang, C.W. Hsu, T.C. Yen, K.J. Lin, H.W. Sung, The glucose-lowering potential of exendin-4 orally delivered via a pH-sensitive nanoparticle vehicle and effects on subsequent insulin secretion in vivo, Biomaterials 32 (2011) 2673–2682.
[22] S. Sajeesh, K. Bouchemal, V. Marsaud, C. Vauthier, C.P. Sharma, Cyclodextrin complexed insulin encapsulated hydrogel microparticles: an oral delivery system for insulin, J. Control. Release 147 (2010) 377–384.
[23] P.H. Johnson, D. Frank, H.R. Costantino, Discovery of tight junction modulators: significance for drug development and delivery, Drug Discov. Today 13 (2008) 261–267.
[24] A. Bernkop-Schnurch, The use of inhibitory agents to overcome the enzymatic barrier to perorally administered therapeutic peptides and proteins, J. Control. Release 52 (1998) 1–16.
[25] C.K. Schauer, O.P. Anderson, Calcium-selective ligands. 2. Structural and spectroscopic studies on calcium and cadmium complexes of EGTA4-[H4EGTA = 3,12-bis(carboxymethyl)-6,9-dioxa-3,12-diazatetradecanedioic acid], J. Am. Chem. Soc. 109 (1987) 3646–3656.
[26] M. Naraghi, T-jump study of calcium binding kinetics of calcium chelators, Cell Calcium 22 (1997) 255–268.
[27] A. Bernkop-Schnurch, Chitosan and its derivatives: potential excipients for peroral peptide delivery systems, Int. J. Pharm. 194 (2000) 1–13.
[28] E. Permyakov, K. Murakami, L. Berliner, On experimental artifacts in the use of metal ion chelators for the determination of the cation binding constants of alpha-lactalbumin. A reply, J. Biol. Chem. 262 (1987) 3196–3198.
[29] T. Matsukawa, S. Ikeda, H. Imai, M. Yamada, Alleviation of the two-cell block of ICR mouse embryos by polyaminocarboxylate metal chelators, Reproduction 124 (2002) 65–71.
[30] R.Y. Tsien, New calcium indicators and buffers with high selectivity against magnesium and protons: design, synthesis, and properties of prototype structures, Biochemistry 19 (1980) 2396–2404.
[31] T. Yamagata, M. Morishita, N.J. Kavimandan, K. Nakamura, Y. Fukuoka, K. Takayama, N.A. Peppas, Characterization of insulin protection properties of complexation hydrogels in gastric and intestinal enzyme fluids, J. Control. Release 112 (2006) 343–349.
[32] F. Madsen, N.A. Peppas, Complexation graft copolymer networks: swelling properties, calcium binding and proteolytic enzyme inhibition, Biomaterials 20 (1999) 1701–1708.
[33] M. Morishita, T. Goto, K. Nakamura, A.M. Lowman, K. Takayama, N.A. Peppas, Novel oral insulin delivery systems based on complexation polymer hydrogels: single and multiple administration studies in type 1 and 2 diabetic rats, J. Control. Release 110 (2006) 587–594.
[34] J. Lee, Intraluminal distension pressure on intestinal lymph flow, serosal transudation and fluid transport in the rat, J. Physiol. 355 (1984) 399–409.
[35] R.C. Brown, T.P. Davis, Calcium modulation of adherens and tight junction function, Stroke 33 (2002) 1706–1711.
[36] E. Roger, F. Lagarce, E. Garcion, J.P. Benoit, Lipid nanocarriers improve paclitaxel transport throughout human intestinal epithelial cells by using vesicle-mediated transcytosis, J. Control. Release 140 (2009) 174–181.
[37] X. Zhao, L. Yin, J. Ding, C. Tang, S. Gu, C. Yin, Y. Mao, Thiolated trimethyl chitosan nanocomplexes as gene carriers with high in vitro and in vivo transfection efficiency, J. Control. Release 144 (2010) 46–54.
[38] R. Vogelmann, W.J. Nelson, Fractionation of the epithelial apical junctional complex: reassessment of protein distributions in different substructures, Mol. Biol. Cell 16 (2005) 701–716.
[39] P. Pulimeno, C. Bauer, J. Stutz, S. Citi, PLEKHA7 is an adherens junction protein with a tissue distribution and subcellular localization distinct from ZO-1 and E-cadherin, PLoS One 5 (2010) e12207.
[40] A.I. Ivanov, A. Nusrat, C.A. Parkos, Endocytosis of epithelial apical junctional proteins by a clathrin-mediated pathway into a unique storage compartment, Mol. Biol. Cell 15 (2004) 176–188.